Estimation of Pure States Using Three Measurement Bases

L. Zambrano,[1,2,*] L. Pereira,[1,2] D. Martínez,[1,2] G. Cañas,[1,3] G. Lima,[1,2] and A. Delgado◉[1,2]

[1]*Instituto Milenio de Investigación en Óptica, Universidad de Concepción, Concepción, Chile*

[2]*Departamento de Física, Facultad de Ciencias Físicas y Matemáticas, Universidad de Concepción, Concepción, Chile*

[3]*Departamento de Física, Universidad del Bío-Bío, Collao 1202, Casilla 5C Concepción, Chile*

We introduce a method to estimate unknown pure d-dimensional quantum states using the probability distributions associated with only three measurement bases. The measurement results of $2d$ projectors are used to generate a set of 2^{d-1} states, the value of the likelihood function of which is evaluated using the measurement results of the remaining d projectors. The state with the highest value of the likelihood function is the estimate of the unknown state. The method estimates all pure states except for a null-measure set, which can be overcome by adapting two bases. The viability of the protocol is experimentally demonstrated using two different and complementary high-dimensional quantum information platforms. First, by exploring the photonic path-encoding strategy, we validate the method on a single eight-dimensional quantum system. Then, we resort to the five-superconducting-qubit IBM quantum processor to demonstrate the high performance of the method in the multipartite scenario.

I. INTRODUCTION

Initially, quantum tomography was motivated by the concept of the quantum state. If a set of probabilities, which is obtained from several different experiments, uniquely characterizes a quantum state, then these probabilities are also a description of the properties of the system. In this case, the quantum state is a convenient mathematical object that summarizes our knowledge about a system in a very concise way but it is not necessarily fundamental. This has led to the design of several tomographic methods. These require the acquisition of information by means of measurements [1,2] and its subsequent postprocessing [3–6]. For a single d-dimensional quantum system, the minimal total number of measurement outcomes required to estimate an unknown state is d^2. Various estimation methods employ a number of measurement outcomes that is equal to or very similar to d^2. Symmetric informationally complete positive operator-valued measures (SIC-POVMs) [7–14] are generalized measurements that allow for the estimation of quantum states with exactly d^2 measurement outcomes. Mutually unbiased bases (MUBs) [15–21] estimate quantum states with $d^2 + d$ measurement outcomes. The existence of SIC-POVMs and MUBs has been proven in

restricted sets of dimensions. For this reason, alternative schemes have been proposed [22–27], which require in the order of d^2 measurement outcomes. In the case of a multipartite system formed by n d-dimensional systems, the total number of measurement outcomes becomes d^{2n}.

In recent decades, however, interest in quantum tomography has shifted from the fundamental to the applied. This is mainly due to the advent of complex quantum devices that exploit the properties of quantum systems to implement information-processing tasks that would be impossible in a reality governed only by classical physics; for example, computing capabilities exponentially faster than any classical machine [28], secure communications via quantum key distribution [29], and metrology beyond the classical limit [30]. The estimation of high-dimensional multipartite quantum states via quantum tomography has become the standard procedure to characterize the performance of complex quantum devices and processes. In this context, the total number of measurement results grows exponentially with the number of parties, which increases the experimental complexity of the data-acquisition process, as well as the computational cost of the optimization problem associated with subsequent data processing. Thereby, the estimation of unknown quantum states of high dimension and the assessment of quantum processes and devices has proven to be a remarkably difficult task from the experimental

*leozambrano@udec.cl

[31–34] and theoretical [35–37] points of view. Thus, the design of better tomographic methods is a contemporary problem.

In order to make the problem of estimating unknown high-dimensional states tractable, the use of *a priori* information has been considered. Thereby, the estimation focuses on a restricted set of states, which allows reduction of the number of measurements [38–41]. Recently, it has been shown [42] that a set of four fixed observables is sufficient to estimate pure quantum states up to a statistically unlikely null-measure set. This set is formed by pure states that, in the canonical basis, have two or more nonconsecutive vanishing coefficients. The addition of a fifth observable, which is diagonal in the canonical basis, helps to determine whether or not a given state belongs to this null-measure set. If this is the case, then the remaining four observables can be adapted to a lower-dimensional subspace. This result is independent of the underlying dimension of the Hilbert space for $d > 4$. In this way, any pure quantum state can be estimated with a total of $5d$ projective measurements (PMs), at most. This estimation procedure involves a simple postprocessing stage and allows the purity assumption to be certified directly from the measurement results. Recently, it has been shown [43] that adaptivity it is not necessary. Five fixed observables estimate all pure quantum states in any dimension, at the expense of a more convoluted construction of the observables and a much more complex postprocessing stage.

Here, we study the estimation of pure quantum states by means of three fixed observables only, that is, with a total of $3d$ PMs. In particular, we show that $2d$ PMs generate a finite set $\mathcal{A}_d$ of 2^{d-1} pure states. Half of the rank-1 projectors come from an observable, while the remaining rank-1 projectors correspond to half of the projectors of each of the remaining two observables. The estimate for the unknown state is given by the state in $\mathcal{A}_d$ with the highest value of the likelihood function, which is evaluated using the measurement results of the remaining d rank-1 PMs. Thus, the costly procedure of optimizing the likelihood function in the complete d-dimensional Hilbert space is reduced to evaluation of the likelihood function in the finite set $\mathcal{A}_d$. The method presented here estimates all pure quantum states except for a null-measure set, which is formed by pure states with consecutive vanishing amplitudes and, according to numerical experiments, pure states with equal amplitudes. This class of states can be detected through the measurements on one base, which allows us to adapt the two resting bases and obtain an estimate. Our numerical experiments do not allow us to rule out the existence of other states that cannot be estimated. Thereby, our method estimates via measurements in three bases, evaluation of the likelihood function, and adaptivity, all pure states with the possible exception of a null-measure set.

Our result is related to a finite-dimensional generalization of the Pauli problem [44]: what is the minimum set of observables that uniquely characterizes a pure state of a quantum system? In the particular case of a spin-s system, it has been shown that measurements of the components of a spin state along two infinitesimally close directions in space (by means of a Stern-Gerlach experiment, for instance) are compatible with 2^{d-1} spin states [45], where the dimension is $d = 2s + 1$. These states can be exhibited explicitly. However, it is necessary that the unknown state does not have zero amplitudes along the measurement directions. It turns out that the expectation value of one additional well-defined operator is enough to single out the actual pure state of the system. This procedure guarantees that the uniqueness of the state is compatible with the measurement. However, it is not constructive [46], that is, it does not provide an explicit determination. In this context, our result corresponds to a constructive procedure that uniquely determines pure states of a d-dimensional quantum system.

We also consider the role of finite statistics effects and show that for moderate ensemble sizes, the present estimation method provides results with an accuracy comparable to that achieved by the five-bases-based pure-state quantum tomographic method.

We demonstrate the experimental feasibility of our estimation method by employing two different and complementary high-dimensional quantum information platforms. First, we estimate the state of an eight-dimensional quantum system that is encoded in the linear transverse momentum of single photons transmitted through difractive apertures generated by spatial light modulators [47–50]. This platform can attain high fidelities for the preparation and measurement of high-dimensional quantum states [51] and therefore its use allows us to properly address the performance of methods for quantum state reconstruction in higher dimensions. In this case, we achieve a high fidelity of 98.5% between the reconstructed state and the prepared one. Then, we study the method in a multipartite scenario and apply it to estimate a two-qubit state generated on the IBM Quantum Experience five-qubit superconducting quantum processor IBMQ-OURENSE. In this case, we are also able to achieve a high fidelity of 96.5%. These results highlight the versatility and high performance of the protocol, indicating that it can be a valuable tool, supporting the development of future quantum technologies dealing with more complex quantum systems [52].

II. REVIEW OF THE FIVE-BASES-BASED PURE-STATE ESTIMATION METHOD

The five-bases-based pure-state quantum tomographic method (5BB-QT) [42] employs PMs onto the canonical

basis $\mathcal{B}_0 = \{|i\rangle\}$ (with $i = 0, \ldots, d-1$) and the bases

$$\mathcal{B}_1 = \left\{ |\varphi_\pm^\nu\rangle_1 = \frac{1}{\sqrt{2}}(|2\nu\rangle \pm |2\nu+1\rangle) \right\},$$

$$\mathcal{B}_2 = \left\{ |\tilde{\varphi}_\pm^\nu\rangle_2 = \frac{1}{\sqrt{2}}(|2\nu\rangle \pm i|2\nu+1\rangle) \right\},$$

$$\mathcal{B}_3 = \left\{ |\varphi_\pm^\nu\rangle_3 = \frac{1}{\sqrt{2}}(|2\nu+1\rangle \pm |2\nu+2\rangle) \right\}, \quad (1)$$

$$\mathcal{B}_4 = \left\{ |\tilde{\varphi}_\pm^\nu\rangle_4 = \frac{1}{\sqrt{2}}(|2\nu+1\rangle \pm i|2\nu+2\rangle) \right\},$$

where $\nu \in [0, (d-2)/2]$. Operations with labels are carried out modulo d. In the case of odd dimensions, the integer part of $(d-2)/2$ is considered and every basis is completed with the state $|d\rangle$. The 5BB-QT method estimates almost any pure state $|\psi\rangle = \sum_{k=0}^{d-1} c_k|k\rangle$ in any dimension d using the set of probability distributions generated by projections on the bases $\mathcal{B}_i$ (with $i = 1, \ldots, 4$). The states that cannot be estimated have at least two nonconsecutive vanishing coefficients. In this case, the system of equations to be solved has infinite solutions. In order to avoid this problem, a fifth basis, the canonical one, is introduced. This is the first basis to be measured and its only purpose is to detect the states that cannot be estimated. If this is the case, the method is adapted by reducing the effective dimension of the estimated state and the bases.

We define $p_\pm^{(k)}$ with k even (odd) as $p_\pm^{(k)} = |\langle\varphi_\pm^k|\psi\rangle|^2$ with $|\varphi_\pm^k\rangle$ in basis $\mathcal{B}_1$ ($\mathcal{B}_3$) and $\tilde{p}_\pm^{(k)}$ with k even (odd) as $\tilde{p}_\pm^{(k)} = |\langle\tilde{\varphi}_\pm^k|\psi\rangle|^2$ with $|\tilde{\varphi}_\pm^k\rangle$ in basis $\mathcal{B}_2$ ($\mathcal{B}_4$). These quantities correspond to transition probabilities from the unknown state toward the states in the bases $\mathcal{B}_i$ and can be experimentally measured. In order to estimate the unknown pure state, the 5BB-QT method employs the set of d equations

$$2c_k c_{k+1}^* = \Lambda_k, \quad (2)$$

with

$$\Lambda_k = (p_+^{(k)} - p_-^{(k)}) + i(\tilde{p}_+^{(k)} - \tilde{p}_-^{(k)}), \quad (3)$$

for $k = 0, \ldots, d-1$. This set of equations can be iteratively solved for the complex probability amplitudes c_k that characterize the unknown state.

III. THE THREE-BASES-BASED PURE-STATE-ESTIMATION METHOD

We can modify the bases (1) in the following way:

$$\mathcal{B}_1 = \left\{ |\varphi_\pm^\nu\rangle_1 = a|2\nu\rangle \pm b|2\nu+1\rangle \right\},$$
$$\mathcal{B}_2 = \left\{ |\tilde{\varphi}_\pm^\nu\rangle_2 = a|2\nu\rangle \pm ib|2\nu+1\rangle \right\},$$
$$\mathcal{B}_3 = \left\{ |\varphi_\pm^\nu\rangle_3 = a|2\nu+1\rangle \pm b|2\nu+2\rangle \right\}, \quad (4)$$

$$\mathcal{B}_4 = \left\{ |\tilde{\varphi}_\pm^\nu\rangle_4 = a|2\nu+1\rangle \pm ib|2\nu+2\rangle \right\},$$

with $|a|^2 + |b|^2 = 1$. In this case, Eq. (2) is still valid. Equation (3) becomes

$$\Lambda_k = \frac{(p_+^{(k)} - p_-^{(k)}) + i(\tilde{p}_+^{(k)} - \tilde{p}_-^{(k)})}{ab}. \quad (5)$$

Using this set of equations, we can estimate pure states. The quantities Λ_k entering into Eq. (5) can be cast in the form

$$\Lambda_k = \left(p_+^{(k)} - \frac{|ac_k|^2 - |bc_{k+1}|^2}{ab} \right) + i\left(\tilde{p}_+^{(k)} - \frac{|ac_k|^2 - |bc_{k+1}|^2}{ab} \right), \quad (6)$$

which is now a function of the probabilities $|c_k|^2$ and $|c_{k+1}|^2$. These are obtained from the measurement on the canonical basis $\mathcal{B}_0$. Equation (6) shows that we only need half the projectors of each basis, plus the values obtained from the canonical basis, to unambiguously estimate the unknown quantum state. The other half of the projectors are redundant because they deliver the same information.

The real, $\text{Re}(\Lambda_k)$, and imaginary, $\text{Im}(\Lambda_k)$, parts of Λ_k are not independent. According to Eq. (2), they are related through the constraint

$$\text{Im}(\Lambda_k)^2 = 4|c_k c_{k+1}|^2 - \text{Re}(\Lambda_k)^2, \quad (7)$$

where the right-hand side is determined by transition probabilities toward the states in $\mathcal{B}_0$ and $\mathcal{B}_1$ (k even) or $\mathcal{B}_3$ (k odd). Therefore, Eq. (7) allows us to determine the value of Λ_k up to a sign without employing the transition probabilities toward the states in the bases $\mathcal{B}_2$ and $\mathcal{B}_4$, that is,

$$\Lambda_{k,\pm} = \text{Re}(\Lambda_k) \pm i|\text{Im}(\Lambda_k)|. \quad (8)$$

All possible sign combinations in the d coefficients Λ_k lead to 2^{d-1} different sets $A_j = \{\tilde{\Lambda}_0, \tilde{\Lambda}_1, \ldots, \tilde{\Lambda}_{d-2}\}$, with $\tilde{\Lambda}_k = \Lambda_{k,+}$ or $\tilde{\Lambda}_k = \Lambda_{k,-}$. Note that Λ_{d-1} is not used, since we have assumed that c_0 is a real positive number. If we solve Eq. (2) for each A_j, we obtain a set $\mathcal{A}_d = \{|\tilde{\psi}^{(k)}\rangle\}$ of 2^{d-1} states ($k = 1, \ldots, 2^{d-1}$). All states in this set are characterized by the same set $\{|_1\langle\varphi_+^\nu|\psi\rangle|^2, |_3\langle\varphi_+^\nu|\psi\rangle|^2, |\langle i|\psi\rangle|^2\}$ of transition probabilities. Thereby, each state in $\mathcal{A}_d$ can be chosen as an estimate of the unknown state $|\psi\rangle$.

In order to resolve the ambiguities in the estimation process, the transition probabilities toward states in bases $\mathcal{B}_2$ and $\mathcal{B}_4$ can be measured. Instead, we propose to replace the

bases $\mathcal{B}_1$ and $\mathcal{B}_3$ by the following modified versions:

$$
\begin{aligned}
\mathcal{B}_1' &= \left\{ |\varphi_+^\nu\rangle_1 = a|2\nu\rangle + b|2\nu+1\rangle, |\varphi_j\rangle_1 \right\}, \\
\mathcal{B}_3' &= \left\{ |\varphi_+^\nu\rangle_3 = a|2\nu+1\rangle + b|2\nu+2\rangle), |\varphi_j\rangle_3 \right\}.
\end{aligned}
\tag{9}
$$

In these new bases, we keep half of the bases that allow us to calculate the real part $\mathrm{Re}(\Lambda_k)$ and add $d/2$ states $|\varphi_j\rangle$ to complete the bases. A possible choice for the bases is

$$
\begin{aligned}
\mathcal{B}_1' &= \left\{ |\varphi_+^\nu\rangle_1 = \frac{1}{\sqrt{2}}(|2\nu\rangle + |2\nu+1\rangle), |\varphi_j\rangle_1 \right\}, \\
\mathcal{B}_3' &= \left\{ |\varphi_+^\nu\rangle_3 = \frac{1}{\sqrt{2}}(|2\nu+1\rangle + |2\nu+2\rangle), |\varphi_j\rangle_3 \right\},
\end{aligned}
\tag{10}
$$

with the states $|\varphi_j\rangle_1$ and $|\varphi_j\rangle_3$ being

$$
|\varphi_j\rangle_1 = \frac{1}{\sqrt{2}} \sum_{m=0}^{1} \sum_{n=0}^{(d-2)/2} (-1)^m \mathcal{F}_{jn} |2n+m\rangle,
\tag{11}
$$

$$
|\varphi_j\rangle_3 = \frac{1}{\sqrt{2}} \sum_{m=0}^{1} \sum_{n=0}^{(d-2)/2} (-1)^m \mathcal{F}_{jn} |2n+m+1\rangle,
\tag{12}
$$

where $\mathcal{F}_{jk}$ is the transformation

$$
\mathcal{F}_{jk} = \frac{1}{\sqrt{d/2}} e^{i[2\pi jk/(d/2)+\phi_k]}.
\tag{13}
$$

The phases ϕ_k are chosen in such a way that the vectors $|\varphi_j\rangle$ provide information about the imaginary parts $\mathrm{Im}(\Lambda_k)$.

In order to select one of the states in $\mathcal{A}_d$ as the estimate $|\tilde{\psi}\rangle$ of $|\psi\rangle$, we resort to maximum-likelihood estimation (MLE), which is a well-known statistical-inference method. MLE is aimed at estimating unknown parameters of a population from observed data [53,54]. The underlying idea is to choose as estimator the maximizer of the probability of obtaining the observed data. Originally, MLE was introduced in the estimation of quantum states [3] due to the fact that the inferred probabilities are affected by errors such as, for instance, finite statistics and experimental errors, which lead to unphysical states. MLE allows us to obtain physically acceptable quantum states.

A quantum system that undergoes a measurement process described by a positive operator-valued measure (POVM), which is described by the set $\{E_i\}$ $(i = 1, \ldots, n)$ of positive semidefinite operators, has a likelihood function $L(\rho)$ given by

$$
L(\rho) = \left(\frac{N!}{\Pi_{j=1}^n n_j} \right) \prod_{i=1}^{n} \mathrm{Tr}(\rho E_i)^{n_i},
\tag{14}
$$

where n_i is number of times that an outcome associated with operator E_i is experimentally registered and $N =$ $\sum_{i=1}^{n} n_i$. If the quantum state prior to the measurement is ρ, then $L(\rho)$ is the total joint probability of registering data $\{n_i\}$. MLE is formulated as the optimization problem

$$
\mathrm{Arg}\left[\max_\rho L(\rho) \right], \text{ such that } \mathrm{Tr}(\rho) = 1 \text{ and } \rho > 0.
\tag{15}
$$

In our case, the POVM describing our estimation method is given by a set $\{E_{i,j}\}$ of $3d$ projectors onto the bases $i = 0, 1, 3$ with $j = 0, \ldots, d-1$. Since measurements on the bases are independent, the likelihood function $L(\rho)$ factorizes as $L_0(\rho)L_1(\rho)L_3(\rho)$ (up to a proportionality constant), where

$$
L_0(\rho) = \prod_{i=0}^{d-1} \mathrm{Tr}(\rho|i\rangle\langle i|)^{n_{0,i}}
\tag{16}
$$

and

$$
L_i(\rho) = L_{i+}(\rho) \prod_j \mathrm{Tr}(\rho|\varphi_j\rangle_i\langle\varphi_j|)^{n_{i,j}},
\tag{17}
$$

with

$$
L_{i+}(\rho) = \prod_\nu \mathrm{Tr}(\rho|\varphi_+^\nu\rangle_i\langle\varphi_+^\nu|)^{n_{i,\nu}},
\tag{18}
$$

for $i = 1, 3$, and the optimization problem is now solved in the set of pure states.

Much of the problem posed by the optimization of the likelihood function is already solved. The full set of states that are compatible with the measurement results of the projections onto states $\{|i\rangle, |\varphi_+^\nu\rangle_1, |\varphi_+^\nu\rangle_3\}$ is $\mathcal{A}_d$. Furthermore, the functions $L_0(\rho)$, $L_{1+}(\rho)$ and $L_{3+}(\rho)$ are constants in $\mathcal{A}_d$. Thereby, MLE reduces to the problem of optimizing

$$
|\tilde{\psi}\rangle = \mathrm{Arg}\left(\max_{|\psi\rangle \in \mathcal{A}_d} L_{\mathrm{red}}(|\psi\rangle\langle\psi|) \right)
\tag{19}
$$

on the discrete set $\mathcal{A}_d$, where we have a reduced likelihood function $L_{\mathrm{red}}(|\psi\rangle\langle\psi|)$ given by

$$
L_{\mathrm{red}}(|\psi\rangle\langle\psi|) = \prod_{i=1,3} \prod_j |\langle\psi|\varphi_j\rangle_i|^{2n_{i,j}}.
\tag{20}
$$

Thus, we need to find the maximum value of $L_{\mathrm{red}}(|\psi\rangle\langle\psi|)$ in the discrete set $\mathcal{A}_d$, which can be done by evaluating $L_{\mathrm{red}}(|\psi\rangle\langle\psi|)$ on each state in $\mathcal{A}_d$.

As in the case of the 5BB-QT method, the three-bases-based pure-state quantum tomographic (3BB-QT) method also requires us to adapt the bases $\mathcal{B}_1'$ and $\mathcal{B}_3'$ in certain cases; in particular, when the unknown state has two or more nonconsecutive vanishing coefficients. These are detected by the measurements carried out on the canonical

basis, in which case $\mathcal{B}'_1$ and $\mathcal{B}'_3$ are adapted to estimate an unknown state belonging to a known lower-dimensional subspace. A similar situation arises due to the use of the likelihood function. There exist states $|\psi\rangle$ with estimates $|\tilde{\psi}^{(k)}\rangle$ that have the same value of the reduced likelihood L_{red}. An extreme example for $a = b = 1/\sqrt{2}$ is the state $|\psi\rangle = (1/\sqrt{d}) \sum_{i=1}^{d} |i\rangle$. In this case, all states $|\tilde{\psi}^{(k)}\rangle$ have the same reduced likelihood. Another example is the state $|\psi\rangle = (1/2)(|1\rangle + i|1\rangle + |1\rangle + i|1\rangle)$. This leads to two sets of states $|\tilde{\psi}^{(k)}\rangle$: each set contains states with the same reduced likelihood. From the results of several numerical experiments, we conjecture that the states with at least two pairs of equal probability amplitudes lead to states $|\tilde{\psi}^{(k)}\rangle$ with the same value of the reduced likelihood. This is a null-measure set. This problem can be mitigated to a great extent by noting that the bases in Eq. (10) are one of many possible choices. The coefficients a and b and the states $|\varphi_j\rangle_1$ and $|\varphi_j\rangle_2$ can be chosen at random. Thus, when the measurement on the canonical basis reveal two or more pairs of equal transition probabilities, coefficients a and b and states $|\varphi_j\rangle_1$ and $|\varphi_j\rangle_3$ are chosen at random and orthogonalized via the Gramm-Schmidt orthogonalization procedure, which generates new bases $\mathcal{B}'_1$ and $\mathcal{B}'_3$ such that the states $|\tilde{\psi}^{(k)}\rangle$ have different values of the reduced likelihood.

Measurement on a fixed set of bases $\{\mathcal{B}_0, \mathcal{B}'_1, \mathcal{B}'_3\}$ together with MLE allows us to estimate most d-dimensional pure states. There are, however, states that cannot be estimated. This is an indication that the bases $\mathcal{B}_0, \mathcal{B}'_1$ and $\mathcal{B}'_3$ do not univocally characterize all pure states, that is, they are not informationally complete. It has been shown that informational completeness at the level of d-dimensional pure states can be achieved with a single POVM composed of $2d$ elements of nonunitary rank [55]. In the rank-1 case, the POVM is composed of no less than $3d - 2$ elements. In the case of orthonormal measurement bases [56], three bases are required to distinguish all pure states in a 2-dimensional Hilbert space. For $d = 3$ and $d \geq 5$, four measurement bases are required. For $d = 4$, the necessary number of bases is three or four. Thus, for $d = 3$ and $d \geq 5$, the use of three bases in our approach leads to a lack of informational completeness, which is consistent with our current results. A fixed set of three bases $\mathcal{B} = \{\mathcal{B}_0, \mathcal{B}'_1, \mathcal{B}'_3\}$ together with MLE is informationally complete within a subset $S_{\mathcal{B}}$ of states of the d-dimensional Hilbert space. When measurements in the canonical base $\mathcal{B}_0$ detect a state $|\psi\rangle$ that cannot be estimated, that is, $|\psi\rangle$ does not belong to $S_{\mathcal{B}}$, then bases $\mathcal{B}'_1$ and $\mathcal{B}'_3$ are updated to a new set of bases $\tilde{\mathcal{B}}$ such that the new subset $S_{\tilde{\mathcal{B}}}$ contains the state $|\psi\rangle$.

IV. ACCURACY OF THE 3BB-QT METHOD

In order to test the estimation accuracy achieved by the 3BB-QT method, we conduct several numerical experiments. As a figure of merit for the accuracy of the estimation process, we employ the infidelity $I(|\psi\rangle, |\tilde{\psi}\rangle)$ between the unknown state and its estimate. This is defined by

$$I(|\psi\rangle, |\tilde{\psi}\rangle) = 1 - |\langle \tilde{\psi} | \psi \rangle|^2. \qquad (21)$$

For infinitesimally close states, the infidelity agrees with the Bures metric [57]. In addition, the inverse of the infidelity can be identified with the sample size required to reach a prescribed accuracy [58]. These two important properties of the infidelity motivate its use. However, it has been shown that states with a small infidelity might lead to very different physical properties [59–61]. Consequently, other accuracy metrics have also been explored, such as, for instance, weighted mean-square error.

We generate a set $\Omega_d = \{|\psi_j\rangle\}$ of $m = 10^5$ unknown pure states, which are identically, uniformly, and independently distributed. The transition probabilities toward the states of each basis are obtained by projecting each member of an ensemble of N identically prepared copies of the unknown state. The transition probabilities are then estimated as

$$|\langle \psi_j | \varphi \rangle|^2 \approx \frac{n_\varphi}{N}, \qquad (22)$$

where $|\varphi\rangle$ is an element of one of the three bases, n_φ is the number of outcomes in the direction of the state $|\varphi\rangle$, and N is the sum of the outcomes of all projections onto the elements of the basis. A total ensemble size of $3N$ is then employed as a resource to obtain an estimate $|\tilde{\psi}\rangle$.

Due to the inherent randomness of the measurement process, the estimation of each state $|\psi_j\rangle$ is simulated $n = 10^2$ times. This leads to n different estimates $|\tilde{\psi}_j^{(i)}\rangle$ (with $i = 1, \ldots, 20$). Thereafter, we average the infidelity over the n estimates, that is,

$$I(|\psi_j\rangle) = n^{-1} \sum_{i=1}^{n} I(|\psi_j\rangle, |\tilde{\psi}_j^{(i)}\rangle). \qquad (23)$$

Finally, we calculate the mean of $I(|\psi_j\rangle)$ in the set of unknown states, that is,

$$\bar{I} = m^{-1} \sum_{j=1}^{m} I(|\psi_j\rangle). \qquad (24)$$

In all numerical simulations, the bases $\mathcal{B}'_1$ and $\mathcal{B}'_3$ are fixed for all states in Ω_d.

Figure 1 displays, on a logarithmic scale for both axes, the mean and median of $I(|\psi_j\rangle)$ as a function of the total ensemble size $3N$ used in the estimation process for a single quantum system with dimension $d = 4$ and for four randomly chosen unknown states in Ω_4 (from top

to bottom) according to a Haar-uniform distribution. The left-hand column compares the mean infidelity generated by the 3BB-QT method (solid red dots) and the IC5BB-QT method [62] (solid blue squares), a variation of the 5BB-QT method that achieves a higher accuracy. For the state in the first row of Fig. 1, we see that the two methods generate almost indistinguishable results. The largest difference in the estimation accuracy is depicted in the third row of Fig. 1, where the IC5BB-QT method delivers an estimation accuracy that is almost one order of magnitude better than the one generated by the 3BB-QT method. The two resting states, shown in the second and fourth rows in Fig. 1, exhibit a small difference in the estimation

accuracies for the two methods. Similar behavior is exhibited by the median of the infidelity, which is depicted in the right-hand column in Fig. 1. Furthermore, the mean and median of $I(|\psi_j\rangle)$ reach very close values in the case of both methods. This is an indication that neither method exhibits outliers in the infidelity distributions.

Figures 2(a) and 2(b) show the mean and median, respectively, of $I(|\psi_j\rangle)$ on Ω_d generated by the 3BB-QT method as a function of the total ensemble size $3N$ for $d = 4$, $d = 8$, and $d = 12$, from bottom to top. A comparison between the two figures reveals a median infidelity located below the mean infidelity for all values of ensemble size and dimension. In particular, the mean infidelity appears to be located at the upper border of the interquartile range. The gap between the median and mean infidelity seems to decrease with an increase of the dimension and to increase with an increase of the ensemble size. The existence of this noticeable gap between the median and the mean infidelity highlights the existence of states that are estimated with a low accuracy with respect to the value of the median.

The 3BB-QT method generates a set Ω_f of estimates that have a set A_j with signs of the imaginary parts of Λ_k that disagree with the unknown state. The states in Ω_f are characterized by an estimation accuracy lower than the mean of $I(|\psi_j\rangle)$ in Ω_d. Figure 3(a) shows the fraction of estimates in Ω_f with respect to a sample of 10^5 unknown states as a function of the total ensemble size in dimension $d = 4$, $d = 8$, and $d = 12$. As the figure indicates, higher dimensions exhibit larger fractions. This can be as large as 0.45 for $d = 12$, that is, almost 45% of all estimates are in Ω_f. Also, the fraction is the largest for small ensemble sizes and rapidly decreases as the ensemble size increases. The average estimation accuracy of estimates in Ω_f is illustrated in Fig. 3(b), where the mean of the infidelity $I(|\psi_j\rangle)$ calculated on the states in the fraction is depicted as a function of the ensemble size in dimension $d = 4$, $d = 8$, and $d = 12$. This set of estimates exhibits a mean that is one order of magnitude higher than the mean of the infidelity on Ω_d. Figure 3(b) also shows the mean of the infidelity $I(|\psi_j\rangle)$ on the complement of Ω_f. This is below the mean infidelity depicted in Fig. 2 for small ensemble sizes. As the ensemble size increases, the mean infidelity $I(|\psi_j\rangle)$ on the complement of Ω_f becomes very close to the mean infidelity on Ω.
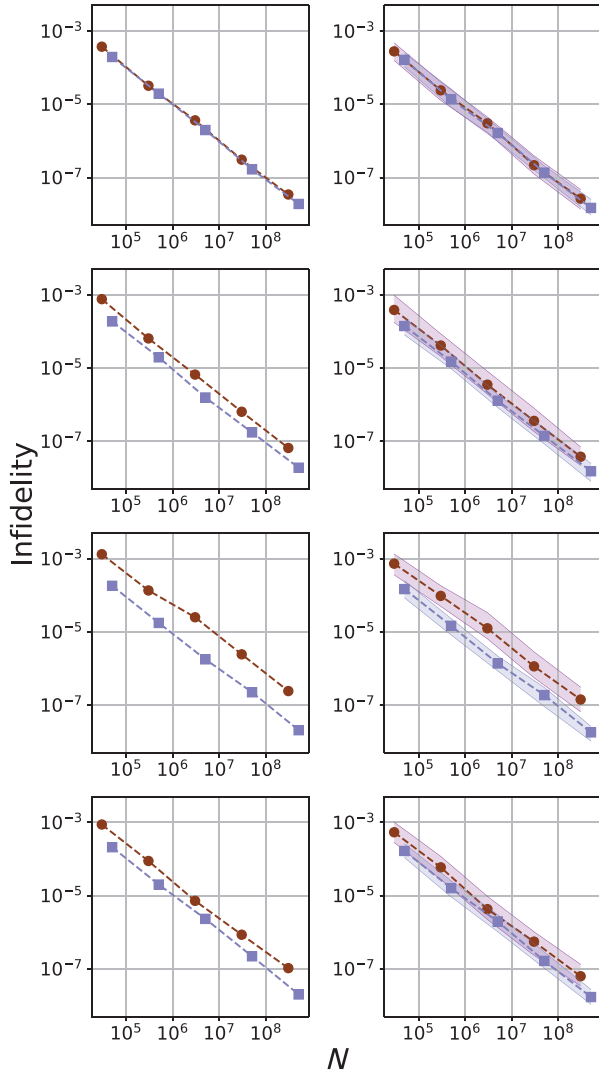

FIG. 1. The left (right) column shows, on a logarithmic scale for both axes, the mean (median) infidelity $I(|\psi_j\rangle)$ as a function of the total ensemble size $3N$ obtained via the IC5BB-QT (solid blue squares) and 3BB-QT (solid red dots) methods for four randomly chosen states in $d = 4$. Shaded areas represent the corresponding interquartile range.

V. EXPERIMENTAL DEMONSTRATION VIA SINGLE-PHOTON PATH-ENCODED QUDITS

To experimentally test the method described in this work, we generate, via the experimental setup illustrated in Fig. 4, an eight-dimensional qudit state encoded into the linear transverse momentum of single photons transmitted by diffractive apertures [47–49]. In this case, the dimension of the qudit state is determined by the number of paths
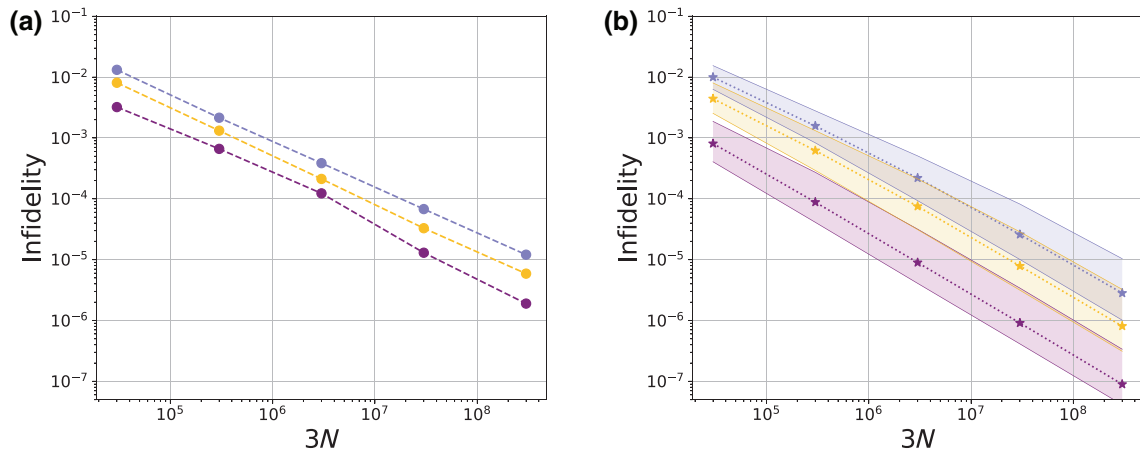
FIG. 2.   The (a) mean (solid dots) and (b) median (solid stars) of $I(|\psi_j\rangle)$ on Ω_d obtained via the 3BB-QT method as a function of the total ensemble size $3N$ (on a logarithmic scale for both axes) for dimensions $d = 4$ (purple), $d = 8$ (yellow), and $d = 12$ (blue), from bottom to top, respectively. The shaded areas represent the corresponding interquartile ranges.

available for the photon transmission over the aperture, which are typically addressed into spatial light modulators (SLMs) [50,63–66]. Here, we define a multislit aperture in the used SLMs with eight parallel slits. Then, the state of the transmitted photons is given by [50]

$$|\psi\rangle = \frac{1}{\sqrt{N}} \sum_{l=-\frac{7}{2}}^{l=\frac{7}{2}} \sqrt{t_l} e^{i\phi_l} |l\rangle, \qquad (25)$$

where $|l\rangle$ represents the state of the photon transmitted by the lth slit, N is a normalization constant, and t_l and ϕ_l are the transmissivity and the relative phase of slit l, respectively.

The setup employed to demonstrate the estimation of an eight-dimensional state is depicted in Fig. 4. This consists of two parts, the state-preparation (SP) stage and the projective-measurement (PM) stage (see Fig. 4). At the SP stage, the photon source is a continuous-wave (cw) laser, operating at 690 nm. It is combined with an acousto-optical modulator (AOM) to generate pulses of 40 ns duration. Then, optical attenuators (not shown in Fig. 4) placed at the output of AOM are used to create weak coherent states. The attenuators are calibrated to set the average number of photons per pulse to $\mu = 0.9$. In this case, the probability of having pulses containing at least one photon is $P(\mu = 0.9|n \geq 1) \approx 59.3\%$. Most of the non-null pulses contain only one photon and represent 61.7% of the experimental runs. This type of light source is typically
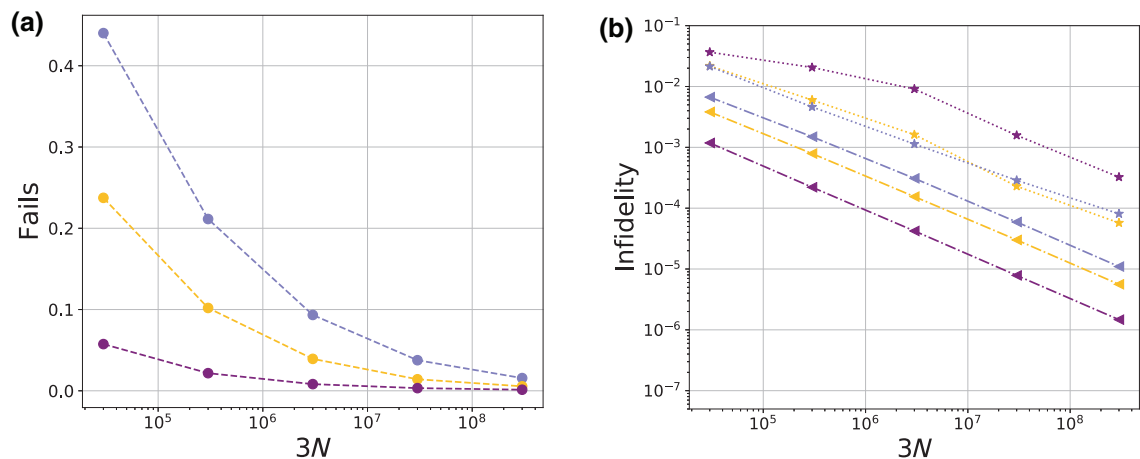

FIG. 3.   (a) A semilogarithmic graph for the fraction of unknown states in the set Ω_f as a function of the ensemble size for dimensions $d = 4$ (solid purple dots), $d = 8$ (solid yellow dots), and $d = 12$ (solid blue dots), from bottom to top. (b) The mean of $I(|\psi_j\rangle)$ on Ω_f (stars, from top to bottom) and on the complement of Ω_f (triangles, from bottom to top) as a function of the total ensemble size $3N$ (on a logarithmic scale for both axes) for dimensions $d = 4$ (purple), $d = 8$ (yellow), and $d = 12$ (blue).
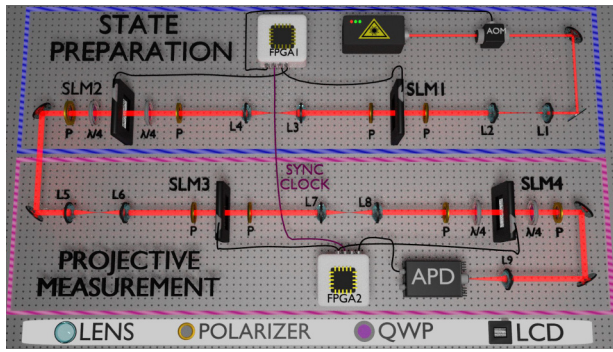
FIG. 4. The experimental setup has two parts, the state-preparation (SP) stage and the projective-measurement (PM) stage. The source consists of a cw laser, an AOM, and calibrated attenuators. The generated single photons are sent through four transmissive SLMs placed in series and with each LCD at the image plane of the previous one. SLM1 and SLM2 are configured to prepare the desired qudit state, which is then is projected onto any qudit state by means of SLM3, SLM4, and an APD. The setup is controlled and synchronized by FPGAs at each stage. See Sec. V for details.

used in quantum information science, since it can be seen as a good approximation to a nondeterministic source of single photons [67–71]. We define a multislit aperture into the used SLMs with eight parallel slits, the width of which is 3 pixels, with a separation of 5 pixels, where each pixel is a square of 32-μm side length.

The generated photons are then sent through a first pair of transmissive SLMs (SLM1 and SLM2). Each SLM is composed of two polarizers, two quarter-wave plates (QWP), and a liquid-crystal display (LCD). By properly configuring the polarizing optics, we set SLM1 and SLM2 to work in amplitude-only and phase-only modulation, respectively [72]. SLM2 is located on the image plane of SLM1 via a 4f system with no magnification. An amplitude (phase) mask with eight slits is generated by SLM1 (SLM2) with the gray levels of each pixel appropriately set to generate the desired initial state. In order to measure over the 3d PMs required by the 3BB-QT method, we employ a second pair of SLMs (SLM3 and SLM4) and a pointlike avalanche photodetector (APD). SLM3 and SLM4 are also configured for amplitude-only and phase-only modulation, respectively. The eight slits addressed onto these last SLMs have the gray level of the pixels adjusted to implement the projections required by the method. The PM is completed with the APD positioned at the center of the transverse Fourier plane of the last lens, $L9$. In this configuration, the single-photon detection rate is proportional to the overlap between the generated and postselected states [65].

During the measurement process, the SP and PM stages run automatically, synchronized and controlled by two field-programmable gate array (FPGA) electronic units at

a rate of 10 Hz. FPGA1 is located at the SP stage and controls the first pair of SLMs and the AOM. In our case, the amplitude and phase masks deployed in the first pair of SLMs remain fixed during all experimental runs to generate the same initial state $|\psi_i\rangle$. In the PM stage, FPGA2 controls the second pair of SLMs and records the number of counts detected by the APD. The synchronization between the two FPGA units allows us to project, for each coherent weak pulse, the prepared initial state into a different state. In order to minimize statistical fluctuations, the experimental setup automatically runs for 10 h.

To test our tomographic method, we consider the quantum state given by the superposition

$$|\psi_i\rangle = \frac{1}{\sqrt{8}}(|0\rangle - |1\rangle + |2\rangle - |3\rangle + |4\rangle - |5\rangle + |6\rangle - |7\rangle),$$
(26)

and measure it using the 3BB-QT bases [i.e., the diagonal basis and the bases of Eq. (10)].

We calculate the probability distributions from the recorded experimental data. With these probability distributions and application of the 3BB-QT method, the infidelity between the estimated state and the target state $|\psi_i\rangle$ is only 0.0156. The state that is experimentally reconstructed is shown in Fig. 5. The upper row shows the real and imaginary parts of the reconstructed density matrix and the lower row shows the real and imaginary parts of the target state. As one can see, the experimental results demonstrate the high performance of the method for reconstructing high-dimensional quantum systems.
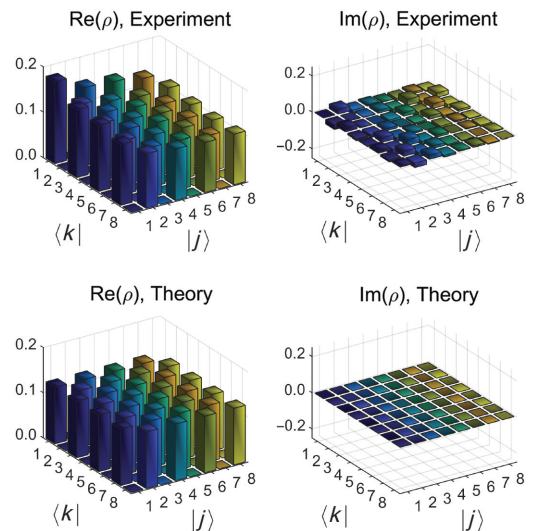

FIG. 5. A comparison between the real and imaginary parts of the matrix coefficients of the experimentally estimated state (upper row), via the experimental setup in Fig. 4, and the single-photon path-encoded eight-dimensional target state of Eq. (26) (lower row).

VI. EXPERIMENTAL ESTIMATION OF TWO-QUBIT STATES IN THE IBM SUPERCONDUCTING QUANTUM PROCESSOR

We also employ the 3BB-QT method to estimate states on the IBM Quantum Experience five-qubit superconducting quantum processor IBMQ-OURENSE. This quantum device has free access via its cloud service. In this quantum processor, we can implement any unitary transformation acting on its qubits. Using QISKIT [73], an open-source development framework for working with quantum computers in PYTHON, we can provide quantum circuits to the quantum processor, which are compiled into an equivalent circuit involving only the machine basis gates. The device only allows measurements on the computational base. Therefore, measuring on a noncomputational basis B requires the application of $B^\dagger$ to a qubit and then measurement of the resulting state on the computational basis. This procedure is repeated a fixed number of times to obtain the required statistics. This, however, introduces noise in the inference of the probabilities that affects the performance of the 3BB-QT. This can be reduced by increasing the number of repetitions. On the other hand, there are systematic errors in the preparations of the gates. Due to the highly nontrivial preparation of the two-qubit controlled-NOT (CNOT) gate, this has an error rate that is much higher than that of the local gates. This is the main source of error that affects the performance of the 3BB-QT method when implemented in the quantum processor.

To reduce the number of CNOT gates in our experiment, we prepare the following randomly chosen separable two-qubit pure state,

$$
\begin{aligned}
|\psi\rangle = {}& 0.5846|00\rangle + (0.157 + 0.295i)|01\rangle \\
& + (0.608 + 0.200i)|10\rangle + (0.062 + 0.362i)|11\rangle,
\end{aligned}
\tag{27}
$$

and measure it using the diagonal base and the bases in Eq. (10). Each one of them corresponds to a different circuit, which we measure using 8192 repetitions for each of them. This leads to a set of probabilities from which we estimate Λ_k in Eq. (6). Afterward, we apply the estimation method. This procedure leads to an infidelity between the estimated state and the target state $|\psi\rangle$ of 0.035, with an average error per gate of 0.005. A comparison between the real and imaginary parts of the density-matrix coefficients of estimate $|\tilde\psi\rangle\langle\tilde\psi|$ and target state $|\psi\rangle\langle\psi|$ is depicted in Fig. 6, where very good agreement can be observed.

VII. CONCLUSIONS

In this paper, we introduce a method to estimate the pure quantum states of d-dimensional quantum systems. The method is based on three measurement bases in any dimension. Thereby, a total of $3d$ PMs are employed. In comparison, the 5BB-QT [42] method requires five observables or, equivalently, $5d$ PMs. The method employs $2d$ PMs to generate a finite set $\mathcal{A}_d$ with 2^{2d-1} pure states. The estimate for the unknown state is given by the state in $\mathcal{A}_d$ with the highest value of the likelihood function. This is evaluated using the measurement results of the remaining d PMs. We emphasize the fact that the likelihood function is evaluated in $\mathcal{A}_d$, which contributes to reducing the computational cost of the method. A set of three fixed measurement bases $\{\mathcal{B}_0, \mathcal{B}'_1, \mathcal{B}'_3\}$ does not allow us to estimate all pure d-dimensional states. States with consecutive vanishing coefficients or equal amplitudes cannot be identified. However, the measurements in $\mathcal{B}_0$ allow us to detect whether or not the unknown state is within this null-measure set. If the unknown state is in the null-measure set, the bases $\mathcal{B}'_1$ and $\mathcal{B}'_3$ can be adapted to allow its estimation. Extensive numerical simulations do not indicated the existence of other classes of state that cannot be estimated. Nevertheless, this possibility cannot be ruled out. Consequently, our method estimates all pure states with the possible exception of a null-measure set.

We also study the estimation accuracy achieved by the 3BB-QT method with the help of the infidelity as an accuracy metric. We show, by means of numerical experiments, that the 3BB-QT method reaches an accuracy similar in median infidelity to that provided by the 5BB-QT method. However, in the case of small ensemble sizes, the mean infidelity provided by the 3BB-QT method is one order of magnitude higher than that reached by the 5BB-QT method. The main reason for this is the fact that the unknown state and its estimate provided by the 3BB-QT
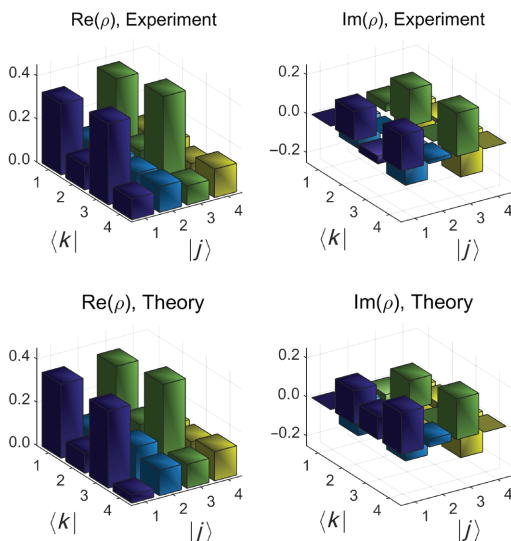

FIG. 6. A comparison between the real and imaginary parts of the matrix coefficients of the experimentally estimated state (upper row), via the IBM superconducting quantum processor, and a randomly chosen two-qubit separable target state (lower row).

method have different signatures of the coefficients $\Lambda_{k,\pm}$. This effect tends to vanish for higher ensemble sizes.

To experimentally prove the effectiveness of the 3BB-QT method, we perform two experiments on different and complementary high-dimensional quantum information platforms. First, we use a photonic platform that relies on the use of programmable spatial light modulators to prepare and measure single eight-dimensional quantum states encoded in the linear transverse momentum of single photons. Due to the high level of precision that can be obtained with the SLMs, the performance of the method can be studied properly and we demonstrate its efficiency by achieving an infidelity of only 1.5% between the prepared and reconstructed state. At the second implementation of the protocol, we use the five-superconducting-qubit IBM quantum processor IBMQ-OURENSE, which serves as a useful tool to study the performance of the method in a multipartite scenario. In this case, the observed infidelity is also very small, at 3.5%. Taken together, these results demonstrate the practicability of the method for the reconstruction of high-dimensional quantum states. Since the number of PMs required is only $3d$, the 3BB-QT method is a powerful and interesting tool for the validation of quantum-based technologies.

ACKNOWLEDGMENTS

---

[1] D. F. V. James, P. G. Kwiat, W. J. Munro, and A. G. White, Measurement of qubits, Phys. Rev. A **64**, 052312 (2001).

[2] R. T. Thew, K. Nemoto, A. G. White, and W. J. Munro, Qudit quantum-state tomography, Phys. Rev. A **66**, 012303 (2002).

[3] Z. Hradil, Quantum-state estimation, Phys. Rev. A **55**, R1561 (1997).

[4] S. M. Tan, An inverse problem approach to optical homodyne tomography, J. Mod. Opt. **44**, 2233 (1997).

[5] M. S. Kaznady, D. F. V. James, Numerical strategies for quantum tomography, Alternatives to full optimization, Phys. Rev. A **79**, 022109 (2009).

[6] R. Blume-Kohout, Optimal, reliable estimation of quantum states, New J. Phys. **12**, 043034 (2010).

[7] E. Prugovečki, Information-theoretical aspects of quantum measurement, Int. J. Theor. Phys. **16**, 321 (1977).

[8] S. T. Flammia, A. Silberfarb, and C. Caves, Minimal informationally complete measurements for pure states, Found. Phys. **35**, 1985 (2005).

[9] J. M. Renes, R. Blume-Kohout, A. J. Scott, and C. M. Caves, Symmetric informationally complete quantum measurements, J. Math. Phys. **45**, 2171 (2004).

[10] T. Durt, C. Kurtsiefer, A. Lamas-Linares, and A. Ling, Wigner tomography of two-qubit states and quantum cryptography, Phys. Rev. A **78**, 042338 (2008).

[11] F. A. Torres-Ruiz, J. Aguirre, A. Delgado, G. Lima, L. Neves, S. Pádua, L. Roa, and C. Saavedra, Unambiguous modification of nonorthogonal single- and two-photon polarization states, Phys. Rev. A **79**, 052113 (2009).

[12] Z. E. D. Medendorp, F. A. Torres-Ruiz, L. K. Shalm, G. N. M. Tabia, C. A. Fuchs, and A. M. Steinberg, Experimental characterization of qutrits using symmetric informationally complete positive operator-valued measurements, Phys. Rev. A **83**, 051801(R) (2011).

[13] N. Bent, H. Qassim, A. A. Tahir, D. Sych, G. Leuchs, L. L. Sánchez-Soto, E. Karimi, and R. W. Boyd, Experimental Realization of Quantum Tomography of Photonic Qudits via Symmetric Informationally Complete Positive Operator-Valued Measures, Phys. Rev. X **5**, 041006 (2015).2160-3308

[14] W. M. Pimenta, B. Marques, T. O. Maciel, R. O. Vianna, A. Delgado, C. Saavedra, and S. Pádua, Minimum tomography of two entangled qutrits using local measurements of one-qutrit symmetric informationally complete positive operator-valued measure, Phys. Rev. A **88**, 012112 (2013).

[15] J. Schwinger, Unitary operator bases, Proc. Natl. Acad. Sci. USA **46**, 570 (1960).

[16] I. D. Ivanovic, Geometrical description of quantal state determination, J. Phys. A **14**, 3241 (1981).

[17] W. K. Wootters and B. D. Fields, Optimal state-determination by mutually unbiased measurements, Ann. Phys. (NY) **191**, 363 (1989).

[18] A. B. Klimov, C. Muñoz, A. Fernández, and C. Saavedra, Optimal quantum-state reconstruction for cold trapped ions, Phys. Rev. A **77**, 060303(R) (2008).

[19] S. N. Filippov and V. I. Man'ko, Mutually unbiased bases: Tomography of spin states and the star-product scheme, Phys. Scr. **2011**, 14010 (2011).

[20] R. B. A. Adamson and A. M. Steinberg, Improving Quantum State Estimation with Mutually Unbiased Bases, Phys. Rev. Lett. **105**, 030406 (2010).

[21] G. Lima, L. Neves, R. Guzmán, E. S. Gómez, W. A. T. Nogueira, A. Delgado, A. Vargas, and C. Saavedra, Experimental quantum tomography of photonic qudits via mutually unbiased basis, Opt. Exp. **19**, 3542 (2011).

[22] L. Pereira, L. Zambrano, J. Cortés-Vega, S. Niklitschek, and A. Delgado, Adaptive quantum tomography in high dimensions, Phys. Rev. A **98**, 012339 (2018).

[23] A. Utreras-Alarcón, M. Rivera-Tapia, S. Niklitschek, and A. Delgado, Stochastic optimization on complex variables and pure-state quantum tomography, Sci. Rep. **9**, 16143 (2019).

[24] L. Zambrano, L. Pereira, S. Niklitschek, and A. Delgado, Estimation of pure quantum states in high dimension at the limit of quantum accuracy through complex optimization and statistical inference, Sci. Rep. **10**, 12781 (2020).

[25] R. Salazar and A. Delgado, Quantum tomography via unambiguous state discrimination, Phys. Rev. A **86**, 012118 (2012).

[26] C. Paiva-Sanchez, E. Burgos-Inostroza, O Jiménez, and A. Delgado, Quantum tomography via equidistant states, Phys. Rev. A **82**, 032115 (2010).

[27] D. Martínez, M. A. Solís-Prosser, G. Cañas, O. Jiménez, A. Delgado, and G. Lima, Experimental quantum tomography assisted by multiply symmetric states in higher dimensions, Phys. Rev. A **99**, 012336 (2019).

[28] S. Debnath, M. M. Linke, C. Figgatt, K. A. Landsman, K. Wright, and C. Monroe, Demonstration of a small programmable quantum computer with atomic qubits, Nature **536**, 63 (2016).

[29] F. Xu, X. Ma, Q. Zhang, H.-K. Lo, and J.-W. Pan, Secure quantum key distribution with realistic devices, Rev. Mod. Phys. **92**, 025002 (2020).

[30] M. Szczykulska, T. Baumgratz, and A. Datta, Multiparameter quantum metrology, Adv. Phys. **1**, 621 (2016).

[31] H. Häffner, W. Hänsel, C. F. Roos, J. Benhelm, D. Chekal-kar, M. Chwalla, T. Körber, U. D. Rapol, M. Riebe, P. O. Schmidt, C. Becher, O. Gühne, W. Dür, and R. Blatt, Scalable multiparticle entanglement of trapped ions, Nature **438**, 643 (2005).

[32] T. Monz, P. Schindler, J. T. Barreiro, M. Chwalla, D. Nigg, W. A. Coish, M. Harlander, W. Hänsel, M. Hennrich, and R. Blatt, 14-Qubit Entanglement: Creation and Coherence, Phys. Rev. Lett. **106**, 130506 (2011).

[33] X. L. Wang, Y. H. Luo, H. L. Huang, M. C. Chen, Z. E. Su, C. Liu, C. Chen, W. Li, Y. Q. Fang, X. Jiang, J. Zhang, L. Li, N. L. Liu, C. Y. Lu, and J. W. Pan, 18-Qubit Entanglement with Six Photons' Three Degrees of Freedom, Phys. Rev. Lett. **120**, 260502 (2018).

[34] M. Gong, M. C. Chen, Y. Z. S. Wang, C. Zha, H. Deng, Z. Yan, H. Rong, Y. Wu, S. Li, F. Chen, Y. Zhao, F. Liang, J. Lin, Y. Xu, C. Guo, L. Sun, A. D. Castellano, H. Wang, C. Peng, C. Y. Lu, X. Zhu, and J. W. Pan, Genuine 12-Qubit Entanglement on a Superconducting Quantum Processor, Phys. Rev. Lett. **122**, 110501 (2019).

[35] M. P. da Silva, O. Landon-Cardinal, and D. Poulin, Practical Characterization of Quantum Devices without Tomography, Phys. Rev. Lett. **107**, 210404 (2011).

[36] J. A. Smolin, J. M. Gambetta, and G. Smith, Efficient Method for Computing the Maximum-Likelihood Quantum State from Measurements with Additive Gaussian Noise, Phys. Rev. Lett. **108**, 070502 (2012).

[37] J. Shang, Z. Zhang, and H. K. Ng, Superfast maximum-likelihood reconstruction for quantum tomography, Phys. Rev. A **95**, 062336 (2017).

[38] M. Cramer, M. B. Plenio, S. T. Flammia, R. Somma, D. Gross, S. D. Bartlett, O. Landon-Cardinal, D. Poulin, and Y. K. Liu, Efficient quantum state tomography, Nat. Comms. **1**, 149 (2010).

[39] D. Gross, Y. K. Liu, S. T. Flammia, S. Becker, and J. Eisert, Quantum State Tomography via Compressed Sensing, Phys. Rev. Lett. **105**, 150401 (2010).

[40] G. Tóth, W. Wieczorek, D. Gross, R. Krischek, C. Schwemmer, and H. Weinfurter, Permutationally Invariant Quantum Tomography, Phys. Rev. Lett. **105**, 250403 (2010).

[41] D. Ahn, Y. S. Teo, H. Jeong, F. Bouchard, F. Hufnagel, E. Karimi, D. Koutný, J. Řeháček, Z. Hradil, G. Leuchs, and L. L. Sánchez-Soto, Adaptive Compressive Tomography with No *a priori* Information, Phys. Rev. Lett. **122**, 100404 (2019).

[42] D. Goyeneche, G. Cañas, S. Etcheverry, E. S. Gómez, G. B. Xavier, G. Lima, and A. Delgado, Five Measurement Bases Determine Pure Quantum States on Any Dimension, Phys. Rev. Lett. **115**, 090401 (2015).

[43] C. Carmeli, T. Heinosaari, M. Kech, J. Schultz, and A. Toigo, Stable pure state quantum tomography from five orthonormal bases, EPL **115**, 30001 (2016).

[44] W. Pauli, in *Die allgemeinen Prinzipien der Wellenmechanik*, edited by H. Geiger and K. Scheel, Handbuch der Physik (Springer, Berlin, 1933), Vol. 24, Pt. 1, p. 98.

[45] S. Weigert, Pauli problem for a spin of arbitrary length: A simple method to determine its wave function, Phys. Rev. A **45**, 7688 (1992).

[46] S. Weigert, How to determine a quantum state by measurements: The Pauli problem for a particle with arbitrary potential, Phys. Rev. A **53**, 2078 (1996).

[47] L. Neves, G. Lima, J. G. Aguirre Gómez, C. H. Monken, C. Saavedra, and S. Pádua, Generation of Entangled States of Qudits Using Twin Photons, Phys. Rev. Lett. **94**, 100501 (2005).

[48] L. Neves, G. Lima, E. J. S. Fonseca, L. Davidovich, and S. Pádua, Characterizing entanglement in qubits created with spatially correlated twin photons, Phys. Rev. A **76**, 032314 (2007).

[49] G. Lima, F. A. Torres-Ruiz, L. Neves, A. Delgado, C. Saavedra, and S. Pádua, Measurement of spatial qubits, J. Phys. B: At. Mol. Opt. Phys. **41**, 185501 (2008).

[50] G. Lima, A. Vargas, L. Neves, R. Guzmán, and C. Saavedra, Manipulating spatial qudit states with programmable optical devices, Opt. Exp. **17**, 10688 (2009).

[51] E. A. Aguilar, M. Farkas, D. Martínez, M. Alvarado, J. Cariñe, G. B. Xavier, J. F. Barra, G. Cañas, M. Pawłowski, and G. Lima, Certifying an Irreducible 1024-Dimensional Photonic State Using Refined Dimension Witnesses, Phys. Rev. Lett. **120**, 230503 (2018).

[52] G. B. Xavier and G. Lima, Quantum information processing with space-division multiplexing optical fibres, Commun. Phys. **3**, 9 (2020).

[53] D. R. Cox, *Principles of Statistical Inference* (Cambridge University Press, New York, 2006).

[54] E. Lehmann and G. Casella, *Theory of Point Estimation* (Springer, New York, 1998).

[55] S. T. Flammia, A. Silberfarb, and C. M. Caves, Minimal informationally complete measurements for pure states, Found. Phys. **35**, 1985 (2005).

[56] C. Carmeli, T. Heinosaari, J. Schultz, and A. Toigo, How many orthonormal bases are needed to distinguish all pure quantum states? Eur. Phys. J. D **69**, 179 (2015).

[57] M. Hübner, Explicit computation of the Bures distance for density matrices, Phys. Lett. A **163**, 239 (1992).

[58] D. H. Mahler, L. A. Rozema, A. Darabi, C. Ferrie, R. Blume-Kohout, and A. M. Steinberg, Adaptive Quantum State Tomography Improves Accuracy Quadratically, Phys. Rev. Lett. **111**, 183601 (2013).

[59] C. Benedetti, A. P. Shurupov, M. G. A. Paris, G. Brida, and M. Genovese, Experimental estimation of quantum discord for a polarization qubit and the use of fidelity to assess quantum correlations, Phys. Rev. A **87**, 052136 (2013).

[60] M. Bina, A. Mandarino, S. Olivares, and M. G. A. Paris, Drawbacks of the use of fidelity to assess quantum resources, Phys. Rev. A **89**, 012305 (2014).

[61] A. Mandarino, M. Bina, C. Porto, S. Cialdi, S. Olivares, and M. G. A. Paris, Assessing the significance of fidelity as a figure of merit in quantum state reconstruction of discrete and continuous-variable systems, Phys. Rev. A **93**, 062118 (2016).

[62] L. Zambrano, L. Pereira, and A. Delgado, Improved estimation accuracy of the 5-bases-based tomographic method, Phys. Rev. A **100**, 022340 (2019).

[63] M. A. Solís-Prosser, M. F. Fernandes, O. Jiménez, A. Delgado, and L. Neves, Experimental Minimum-Error Quantum-State Discrimination in High Dimensions, Phys. Rev. Lett. **118**, 100501 (2017).

[64] W. M. Pimenta, B. Marques, M. A. D. Carvalho, M. R. Barros, J. G. Fonseca, J. Ferraz, M. Terra Cunha, and S. Pádua, Minimal state tomography of spatial qubits using a spatial light modulator, Opt. Exp. **18**, 24423 (2010).

[65] S. Etcheverry, G. Cañas, E. S. Gómez, W. A. T. Nogueira, C. Saavedra, G. B. Xavier, and G. Lima, Quantum key distribution session with 16-dimensional photonic states, Sci. Rep. **3**, 2316 (2013).

[66] Q. P. Stefano, L. Rebón, S. Ledesma, and C. Iemmi, Determination of any pure spatial qudits from a minimum number of measurements by phase-stepping interferometry, Phys. Rev. A **96**, 062328 (2017).

[67] N. Gisin, G. Ribordy, W. Tittel, and H. Zbinden, Quantum cryptography, Rev. Mod. Phys. **74**, 145 (2002).

[68] H. K. Lo, M. Curty, and K. Tamaki, Secure quantum key distribution, Nat. Photon. **8**, 595 (2014).

[69] E. Diamanti, H. K. Lo, B. Qi, and Z. Yuan, Practical challenges in quantum key distribution, npj Quantum Inf. **2**, 16025 (2016).

[70] F. Xu, X. Ma, Q. Zhang, H. K. Lo, and J. W. Pan, Secure quantum key distribution with realistic devices, Rev. Mod. Phys. **92**, 025002 (2020).

[71] S. Pirandola, U. L. Andersen, L. Banchi, M. Berta, D. Bunandar, R. Colbeck, D. Englund, T. Gehring, C. Lupo, C. Ottaviani, J. Pereira, M. Razavi, J. S. Shaari, M. Tomamichel, V. C. Usenko, G. Vallone, P. Villoresi, and P. Wallden, Advances in Quantum Cryptography, arXiv:1906.01645.

[72] I. Moreno, P. Velásquez, C. R. Fernández-Pousa, M. M. Sánchez-López, and F. Mateos, Jones matrix method for predicting and optimizing the optical modulation properties of a liquid-crystal display, J. Appl. Phys. **94**, 3697 (2003).

[73] QISKIT can be accessed at https://qiskit.org.